Magneto-optical investigations of Eu-based diluted magnetic lead chalcogenides

F. Geist, W. Herbst, C. Mejía-García, H. Pascher, and R. Rupprecht
Experimentalphysik I, Universität Bayreuth, D-95440 Bayreuth, Germany

Y. Ueta, G. Springholz, and G. Bauer
Semiconductor Physics Group, Universität Linz, A-4040 Linz, Austria

M. Tacke
Fraunhofer Institut für Physikalische Meßtechnik, D-79110 Freiburg, Germany
(Received 2 January 1997; revised manuscript received 6 August 1997)

MBE grown $Pb_{1-x}Eu_xTe$ and $Pb_{1-x}Eu_xSe$ films with Eu contents up to 7% were investigated by various magneto-optical methods as interband absorption, photomodulated reflectivity, photoluminescence, and coherent anti-Stokes Raman scattering (CARS) in the midinfrared. The observed interband and intraband transition energies were interpreted in the framework of the Mitchell and Wallis band-structure model with the exchange interaction taken into account in mean-field approximation. The interband matrix elements of the selenide are independent of the Eu concentration up to $x=0.07$, whereas in the telluride they are reduced by about a factor of 2 between $x=0$ and 0.05. The signs and the magnitudes of the exchange parameters for the exchange interaction between the free carriers in the conduction and valence band, respectively, and the localized magnetic moments of the Eu^{2+} ions are similar in $Pb_{1-x}Eu_xTe$ and $Pb_{1-x}Eu_xSe$. This implies that in $Pb_{1-x}Eu_xTe$ the exchange interaction decreases the spin splitting of the valence band as it is known from $Pb_{1-x}Eu_xSe$. The sign and magnitude of the exchange parameters are different from the Mn-based compounds indicating that the effect is dominated by the hybridization of the band states with the localized wave functions of the $4f$ or $3d$ electrons, respectively. The minima of the magnetoabsorption spectra exhibit a strong line broadening with increasing Eu concentration. Weaker transitions are no longer observable. Thus for higher Eu contents CARS turned out to be important not only for the determination of exchange parameters but also for the precise determination of the anisotropy of the interband matrix elements. With increasing x a strong decrease of the matrix elements is observed in the telluride, whereas the matrix elements in the selenide are less influenced. [S0163-1829(97)01044-8]

I. INTRODUCTION

Alloying lead chalcogenides with Eu strongly opens the energy gap. Quantum wells composed of these alloys with the respective binary compounds are of type I in contrast to, e.g., Mn-based systems. This fact makes the Eu alloys particularly interesting for laser diodes emitting in the midinfrared.[1–4] For a systematic control of the device parameters a detailed knowledge of the band structure is important.

Moreover the diluted magnetic compounds are interesting due to the exchange interaction between free carriers and the localized magnetic moments of the paramagnetic Eu^{2+} ions. For rather low Eu contents, in the past precise band and exchange parameters have been obtained.[5–9] Concerning the interband matrix elements of $Pb_{1-x}Eu_xTe$ there was some controversy in the literature.[10,11]

In the present investigation the range of Eu concentrations in $Pb_{1-x}Eu_xTe$ and $Pb_{1-x}Eu_xSe$ is up to 7%. A combination of a variety of experimental methods as interband magnetoabsorption, photomodulated reflectivity, photoluminescence, and coherent anti-Stokes Raman scattering is used to observe inter as well as intraband transitions. This allows a precise characterization of the band structure.

II. BAND MODEL

A. Nonmagnetic host material

The band structure of PbTe and PbSe is characterized by small direct energy gaps at the L points of the Brillouin zone, which results in a many-valley structure with a strong anisotropy of about 10 of the effective masses of valence and conduction band in PbTe and less (approximately 2) in PbSe. The Landau-level energies can be calculated within the $\mathbf{k}\cdot\mathbf{p}$ band model according to Mitchell and Wallis.[12] This treatment describes the interaction between the lowest conduction and the highest valence band exactly taking into account the two higher conduction and two lower valence bands in perturbation up to order k^2. This approximation is justified, because the energy difference between the so-called far bands and the lowest conduction band and highest valence band is about 2 eV (Ref. 13) and the energy gaps of the investigated samples are smaller than 400 meV.

Deviations from this model are expected for energies which are much higher than the energy gaps. Such discrepancies are indeed observed in intraband magnetoabsorption in PbTe and PbSe (Refs. 14 and 15) at very high magnetic fields and temperatures up to 300 K and from photomodulated reflectivity measurements in PbTe for $\hbar\omega > 2E_g$.[16] In this respect the analysis of our experiments within the Mitch-

ell and Wallis model is restricted to lower energies within the energy bands and not too high Eu contents. Then the Landau level energies can be obtained by diagonalization of a 4×4-matrix Hamiltonian.[17]

With higher Eu concentrations the gap is opened that far that the $4f$ levels of the Eu^{2+} ions are no longer within the valence band but are located in the forbidden gap[18,19] drastically changing the observed inter- and intraband transitions. This is another reason why we limited ourselves to Eu contents smaller than 5% in the telluride and 7% in the selenide.

B. Exchange interaction in diluted magnetic alloys

The band structure of the diluted magnetic semiconductors $Pb_{1-x}Eu_xTe$ and $Pb_{1-x}Eu_xSe$ can be calculated in the vicinity of the direct gaps by a modified $\mathbf{k}\cdot\mathbf{p}$ band model, which takes into account the exchange interaction between the free carriers and the magnetic moments of the electrons of the half-filled $4f$ shell in the Eu^{2+} ions. This effect was studied by several authors[20,21] and the results are reviewed by Bauer, Pascher, and Zawadzki.[7] In a mean-field approximation the exchange matrix [see Ref. 7: Eq. (35) multiplied with the Brillouin function Eq. (42)] is added to the 4×4 Hamiltonian of the diamagnetic host crystal. The exchange interaction is proportional to a modified Brillouin function describing the magnetization of the semimagnetic semiconductor and an exchange matrix with the elements a, b, c, and d defined in Refs. 7 and 21. The matrix elements are functions of the four exchange parameters A, a_1 (valence band) and B, b_1 (conduction band) (see Ref. 7).

The off-diagonal exchange terms c and d are responsible for a strong coupling of Landau states with different quantum numbers for $\Phi\neq0°$ (angle between magnetic-field direction and valley axis). For this reason the 4×4 matrix must be extended to an infinite Hamiltonian which one has to truncate in order to calculate the eigenenergies of a limited number of Landau levels. The exact Hamiltonian is taken from Bauer, Pascher, and Zawadzki.[7]

From the exchange parameters and the spin-orbit mixing parameters the four exchange integrals can be calculated.[21,22] In the *tellurides* the exchange integrals are defined as

$$\frac{1}{\Omega_0}\langle R|J|R\rangle=\alpha=\frac{a_1}{\cos^2\Theta^+},$$

$$\frac{1}{\Omega_0}\langle S_\pm|J|S_\pm\rangle=\delta=\frac{a_2}{\sin^2\Theta^+},$$

$$\frac{1}{\Omega_0}\langle Z|J|Z\rangle=\beta_\perp=\frac{b_1}{\sin^2\Theta^-},$$

$$\frac{1}{\Omega_0}\langle X_\pm|J|X_\pm\rangle=\beta_\parallel=\frac{b_2}{\cos^2\Theta^-}. \tag{1}$$

In PbSe and PbTe the conduction band shows a different band-edge symmetry.[12,13] Hence in the definition of $\beta_\perp$ and $\beta_\parallel$ in the case of the selenides $\sin^2\Theta^-$ has to be replaced by $\cos^2\Theta^-$ and vice versa.

With increasing Mn or Eu content an antiferromagnetic coupling between neighboring magnetic ions can occur. The coupling constant J_{NN} for this exchange interaction is about 2.5 K in the Mn-based lead chalcogenides and about 0.25 K in $Pb_{1-x}Eu_xTe$ (Ref. 23) and in $Pb_{1-x}Eu_xSe$.[24] According to a statistical distribution of the paramagnetic ions in the host lattice, about $(1-x)^{12}$ of the ions are located in pairs and do, in the case of Mn^{2+}, not contribute to the macroscopic magnetization taking into account their strong antiferromagnetic coupling.[25,26] For this reason a strong decrease of the effective spin S_0 with increasing x is observed in magnetization measurements in $Pb_{1-x}Mn_xSe$ and $Pb_{1-x}Mn_xTe$.[23,27,28] Due to the much smaller coupling constants in the Eu-based lead chalcogenides with concentrations up to 5% no significant decrease of S_0 is found in magnetization experiments.[29,30] The coupling between interacting magnetic ions is considered by a second parameter T_0 in the modified Brillouin function. After Spalek *et al.*[31] this characteristic temperature scales linearly with x and depends on the coupling constant J_{NN}.

For the band-structure calculations the energy gap E_g and the interband matrix elements $2P_\perp/m_0^2$ and $2P_\parallel/m_0^2$ are fitted to magneto-optical interband and coherent anti-Stokes Raman scattering (CARS) data. The far band parameters are taken from PbTe and PbSe, respectively. Due to the small coupling constant J_{NN} in the Eu compounds we assumed that the effective spin S_0 is unchanged. The effective temperature T_0 can be fitted to the CARS data at $T=1.8$ K, but only for $x>5\%$ T_0 is significantly larger than 0 K.

Calculated Landau levels for $Pb_{1-x}Eu_xSe$ are shown in Fig. 4 of Ref. 7. The primary effect of the exchange interaction between the localized magnetic moments of the Eu^{2+} ions and the free carriers is the modification of the spin splittings in the valence and conduction band. Because of this exchange interaction the Landau levels exhibit a Brillouin function like bending, especially in the valence band. The band structure of $Pb_{1-x}Eu_xTe$ is rather similar, except the larger anisotropy of the telluride compared to the selenide.

In contrast to $Pb_{1-x}Mn_xTe$ or $Pb_{1-x}Mn_xSe$ the spin splitting in the Eu compounds [see full lines in Fig. 7(b)] is reduced in the valence band, so that in samples with higher Eu contents the spin splitting even changes its sign in the investigated range of the applied magnetic fields. The step occurring for the spin-flip transition of $\Phi=35°$ valley in the valence band is due to a strong mixing and anticrossing of states. This occurs in $Pb_{1-x}Eu_xSe$ too, however, for $x=0.042$ in a magnetic-field range of about 3.4 T [see Fig. 8(a)]. For a comparable Eu content the effect is more pronounced in the telluride. Due to the larger gap of the telluride the host g factor is smaller and the relative strength of the exchange interaction is stronger. Since the exchange integrals are smaller in the Eu-based lead chalcogenides than in the Mn-based compounds,[22,32] samples with higher Eu content than in the case of Mn^{2+} have to be investigated to obtain reliable exchange parameters. On the other hand, a higher Eu content strongly opens the energy gap and affects the interband matrix elements.

C. Calculation of the magnetotransmission

If the line broadening due to scattering is small, then interband transition energies between Landau levels are obtained straight forward from the transmission minima. With

TABLE I. Sample parameters of $Pb_{1-x}Eu_xSe$.

Identification	E_g (meV)	x (from E_g)	d (μm)	$N_{n,p}^{(77\,K)}$ (10^{17} cm^{-3})	$\mu^{(77\,K)}$ (cm^2/V s)
I	181.1	0.012	2		
II	189.1	0.014	2	$\sim +1$	$5..10\cdot 10^3$
III	219.0	0.024	2		
IV	264.3	0.039	6		
V	273.4	0.042	10	+0.48	4620
VI	354.5	0.069	11	+0.37	979

increasing Eu content the relaxation time τ is decreased, resulting in a strong level broadening. Then a model calculation of the transmission is necessary to understand the experimental interband absorption spectra.

The dependence of the transmitted intensity at fixed photon energy as a function of the magnetic field is calculated by the following procedure:

(i) Calculation of interband transition energies for an array of magnetic fields by diagonalization of the Mitchell and Wallis $\mathbf{k}\cdot\mathbf{p}$ Hamiltonian.

(ii) For each of the magnetic fields the imaginary part of the dielectric function is calculated according to Roth *et al.*[33,34]

$$\varepsilon_2(\omega)\propto\sum_{\Phi} A(\Phi)\,\frac{B}{\omega^2}\,\sqrt{m_B^{\mathrm{red}}(\Phi)}\,|P_B(\Phi)|^2 \times\sum_n\left[\frac{\omega-\omega_n+\left((\omega-\omega_n)^2+\frac{1}{\tau^2}\right)^{1/2}}{2\left((\omega-\omega_n)^2+\frac{1}{\tau^2}\right)}\right]^{1/2}, \quad (2)$$

where $\Sigma_\Phi A(\Phi)$ symbolizes the sum over all valleys. $m_B^{\mathrm{red}}(\Phi)$ denotes the reduced effective mass of conduction and valence band with $m_B^{\mathrm{CB,VB}}(\Phi)=m_\parallel^{\mathrm{CB,VB}}\cos^2\Phi+m_\perp^{\mathrm{CB,VB}}\sin^2\Phi$ and $P_B(\Phi)$ is the interband matrix element for the respective angle between the valley axis and the direction of the magnetic field,

$$|P_B(\Phi)|^2=\frac{m_0}{2}\left(\frac{2P_\perp^2}{m_0}\right)\sqrt{\cos^2\Phi+(P_\perp/P_\parallel)^{-2}\sin^2\Phi}. \quad (3)$$

The last term in Eq. (2) denotes the combined density of states with the interband transition energies $\hbar\omega_n$ and the linewidth characterized by the relaxation time τ for these transitions. The Dingle temperature is then defined as $T_D=(\hbar/2\pi k_B\tau)$.[34]

(iii) Calculation of the real part $\varepsilon_1(\omega)$ from $\varepsilon_2(\omega)$ by Kramers Kronig transformation for each $\mathbf{B}$ value. $\varepsilon_1^t(\omega)=\varepsilon_1(\omega)+\varepsilon_1^{\mathrm{bg}}(\omega)$, with $\varepsilon_1^{\mathrm{bg}}(\omega)$ being a phenomenological background to the total real part of the dielectric constant.[35]

(iv) $\varepsilon_1^t(\omega)$ and $\varepsilon_2(\omega)$ yield the transmission and the reflectivity of the epitaxial film taking into account multiple reflections at the film surfaces including interference effects.

These calculations are performed as a function of ω for at least 100 magnetic field values between 0 and 7 T. From the array of results the transmission at fixed ω as a function of the magnetic field $|\mathbf{B}|$ can be extracted.

III. EXPERIMENT

A. Samples

The samples were grown by molecular-beam epitaxy on cleaved BaF_2 substrates with [111] direction perpendicular to the sample surface. The Eu contents, film thicknesses, carrier densities, and Hall mobilities are listed in Tables I and II. The Eu concentrations in the $Pb_{1-x}Eu_xSe$ samples were determined from the energy gaps using the dependence of E_g on x:[3]

$$E_g(\mathrm{meV})=146.3+3000x \quad \text{for } Pb_{1-x}Eu_xSe. \quad (4)$$

In the case of $Pb_{1-x}Eu_xTe$ the Eu content was determined by x-ray scattering and a chemical analysis based on atom absorption spectroscopy. For the dependence of E_g on x for $T\rightarrow 0$ an expression similar to Eq. (4) is obtained which is in agreement with published data of Ishida *et al.*[36]

$$E_g(\mathrm{meV})=189.7+4480x \quad \text{for } Pb_{1-x}Eu_xTe. \quad (5)$$

The factors dE_g/dx are only valid for x up to 0.05 in $Pb_{1-x}Eu_xTe$ and for $x<0.07$ in $Pb_{1-x}Eu_xSe$ due to the above-mentioned location of the $4f$ levels of the Eu^{2+} ions.

B. Magneto-optical interband transitions

The interband transition energies are determined by magnetoabsorption of the epitaxial films in Faraday ($\mathbf{k}\|\mathbf{B}\|[111]$) and Voigt geometry ($\mathbf{k}\perp\mathbf{B}\|[110]$). Because of the wide range of energy gaps we used a CO-laser, a frequency doubled CO_2-laser, a dye laser together with a Raman-shifter or a globar as light sources. In Faraday configuration with circularly polarized light, interband transitions from the conduction to the valence band with $\Delta n=0$ and $\Delta s=\pm 1$ are

TABLE II. Sample parameters of $Pb_{1-x}Eu_xTe$.

Identification	E_g (meV)	x (from E_g)	d (μm)	$N_{n,p}^{(77\,K)}$ (10^{17} cm^{-3})	$\mu^{(77\,K)}$ (cm^2/V s)
A	207.7	0.0040	4.0	*n* type	
B	222.0	0.0072	3.4	−1.3	21000
C	228.2	0.0086	4.6	−4.4	15000
D	252.6	0.0140	3.03	+1.4	3190
E	267.8	0.017	3.8	−1.0	9000
F	309.4	0.027	4.29	−0.11	3080
G	343.8	0.034	4.8	+0.59	1790
H	345.2	0.035	4.2	−1.6	
J	395.9	0.046	4.01	−2.45	1997

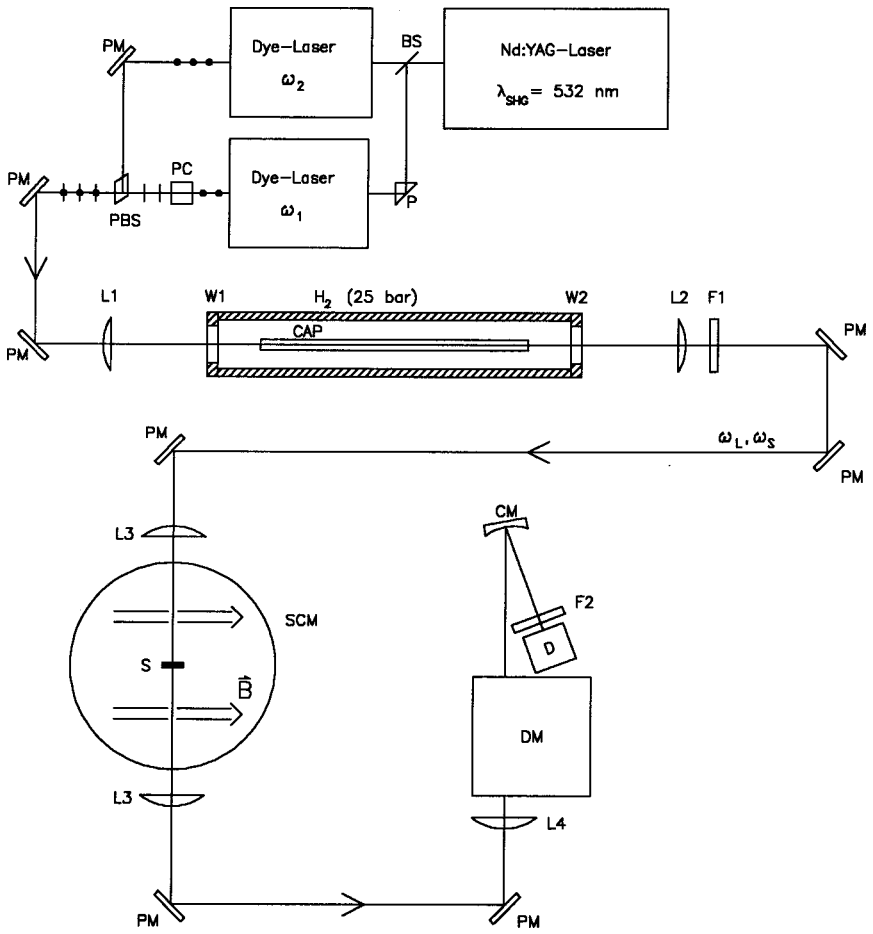

FIG. 1. Experimental setup of the CRS with the Raman shifter in the midinfrared [$\omega_{L,S}=\omega_{1,2}-3\times4155$ (cm^{-1}) according to Ref. 39]. BS coated beam splitter; P: suprasil prism; PC: pockels cell; PM: plane mirror; PBS: polarizing beam splitter ($CaCO_3$ prism); $L1$: suprasil lens ($f=300$ mm); $W1$: suprasil window; CAP: glass capillary ($\varnothing=0.7$ mm; $l=700$ mm); $W2$: CaF_2-window; $L2$: CaF_2 lens ($f=300$ mm); $F1$: Si and/or Ge filter; $L3$: BaF_2-lens ($f=300$ mm); S: sample ($T=1.7...300$ K); SCM: superconducting magnet ($B<7$ T); $L4$: BaF_2 lens ($f=100$ mm); M: double monochromator; CM: concave mirror ($f=200$ mm); $F2$: Si-, Ge-, or InAs filter; D: photovoltaic InSb detector.

the strongest allowed transitions. Because of the many-valley structure, transitions in one valley with $\Phi=0°$ and in three valleys with $\Phi=70.53°$ can be observed. In Voigt configuration with an $\mathbf{E}\|\mathbf{B}$ interband transitions with $\Delta n=0$ and $\Delta s=0$ are observed for two valleys with $\Phi=35.26°$ and 90°, respectively. From the differences of the transition energies in Faraday and Voigt geometry the spin splittings could be determined, in principle, but the experimental errors are rather large because the spin splittings and the influence of the exchange interaction are much smaller than interband transition energies.

In homogeneous PbSe as well as PbTe the g factors of valence and conduction bands are almost identical. Consequently σ^+ and σ^- polarized interband transitions occur at the same magnetic field. Due to the difference of the exchange interaction in valence and conduction bands, the degeneracy of σ^+ and σ^- transitions is lifted in $Pb_{1-x}Eu_xSe$ [see Fig. 8(c) of Ref. 7]. From the polarization selection rules and the fact that the σ^+ polarized transitions occur at smaller magnetic fields it can be deduced that the spin splitting in the valence band is smaller than in the conduction band. In this way the interband transitions are important for CARS experiments, which very exactly determine the absolute value of the effective g factor but not the sign.

From the interband magneto-optical data mainly the two-band parameters E_g, $2P_\perp^2/m_0$, and $P_\perp/P_\parallel$ are fitted. However, in the cases where due to a broad linewidth interband absorption is only observed with one valley orientation, CARS data are important for the determination of matrix elements, too. Exchange parameters can only be found exactly from spin flip transitions observed by CARS. The far band parameters are assumed to be the same as in PbSe and PbTe, respectively, an assumption justified by the small x values of less than 7%.

C. Coherent Raman scattering

Spin resonances of electrons and holes in semiconductors are Raman allowed transitions. Due to the small penetration depths of visible light in narrow gap semiconductors conventional Raman-scattering experiments do not work. Since infrared detectors are much less sensitive than photomultipliers or CCD (charge coupled device) detectors, spontaneous Raman scattering in the mid- infrared is only observable under very special conditions.[37] Coherent Raman methods like CARS, however, turned out to be very powerful and universally applicable to the observation of spin-flip transitions.[38,39] In order to measure directly the temperature and magnetic-

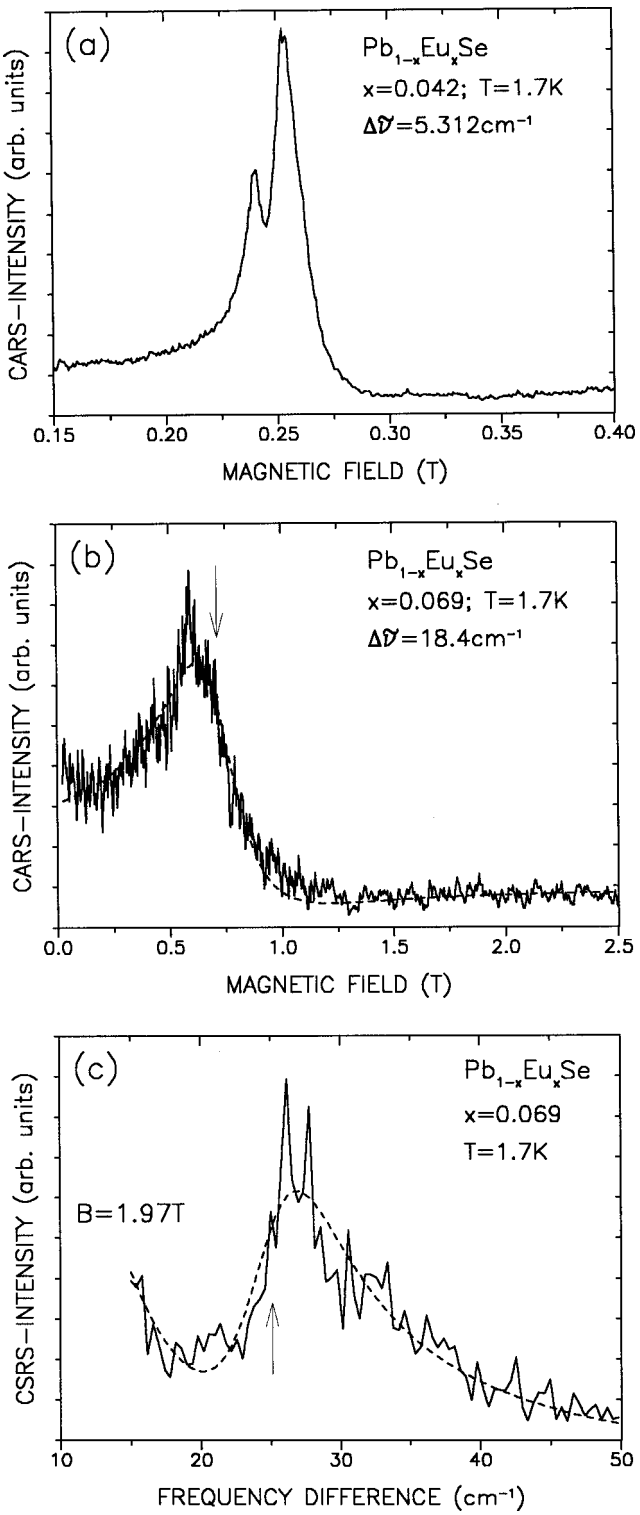

FIG. 2. CARS intensity of $Pb_{1-x}Eu_xSe$ with $x=0.042$ (a) and $x=0.069$ (b) as a function of the magnetic field for $T=1.7$ K for constant frequency differences $\Delta\tilde{\nu}$. (c) CSRS intensity of $Pb_{1-x}Eu_xSe$ with $x=0.069$ vs the frequency difference $\Delta\tilde{\nu}$ for $T=1.7$ K at a fixed magnetic field ($B=1.97$ T). The arrows in (b) and (c) denote the resonance positions obtained by line-shape fitting (dashed lines).

field dependence of the electron and hole g factors, a setup for CARS experiments operating in the infrared was used.

In the experiments described in the present article resonance CARS was used with the laser frequencies nearly corresponding to the energy gaps of the investigated materials. The method yields signals with signal to noise ratios considerably improved with respect to nonresonant CARS applied in previous investigations (e.g., Ref. 7). This results in a larger number of observable transitions entering the band- and exchange parameter fits and consequently more precise results. In order to take advantage of band-gap resonances of the CARS signal in samples with rather different energy gaps we used alternatively two CO_2 lasers[40] or their second harmonic,[39] or two visible dye lasers together with one H_2-Raman shifter[41] to generate infrared radiation with frequencies ω_L and ω_S, respectively (see Fig. 1). Due to the 700-mm-long waveguide the beams with the two frequencies are exactly collinear. They are focused onto the sample which is held in Voigt configuration in a variable temperature cryostat in a superconducting magnet. The double monochromator serves as a broadband filter which suppresses the laser light. The beams with frequencies ω_L and ω_S generate in the sample radiation with new frequencies by optical four wave mixing. Among these, the frequency $\omega_{AS}=2\omega_L-\omega_S$ corresponds to the anti-Stokes frequency (CARS) and $\omega_{SS}=2\omega_S-\omega_L$ to the second Stokes frequency (CSRS) of a conventional Raman-scattering experiment with pump laser at ω_L and Raman shift $\omega_L-\omega_S$. The spectra at ω_{AS} and ω_{SS} are almost similar and yield the same information on the Raman allowed transitions. But in the case of resonant CARS with $\hbar\omega_L \geqslant E_g$, the generated anti-Stokes intensity ($\omega_{AS}>\omega_{SS}$) is reduced more by one-photon absorption. On the other hand, the radiation with the frequency ω_{SS} may be superposed by a strong photoluminescence, so that only CARS will be applicable.

The intensity at ω_{AS} or ω_{SS} is monitored either as a function of magnetic field $|\mathbf{B}|$ for several fixed combinations ω_L and ω_S or alternatively as a function of $\omega_L-\omega_S$ with fixed $|\mathbf{B}|$. The latter method is particularly important for the observation of transitions which do not exhibit a significant dependence on the magnetic field [see, e.g., the spin resonance in the valence band in Fig. 8(b) for $B>2$ T or valence-band resonances around $B=1$ T in Fig. 8(a)].

The intensity I_{AS} at ω_{AS} is proportional to the square of the nonlinear susceptibility $\chi^{(3)}$, which is resonantly enhanced whenever $\omega_L-\omega_S$ corresponds to the transition energy of a Raman allowed transition. In a magnetic field with orientation $\mathbf{B}\perp\mathbf{k}$, i.e., in Voigt geometry, the strongest one is a spin-flip resonance if

$$\hbar(\omega_L-\omega_S)=\hbar\Delta\omega=g^*\mu_B B_{res}, \tag{6}$$

where g^* is the effective g factor for the particular orientation of $\mathbf{B}$.

In the CRS experiments complicated line shapes occur due to the interference of the resonant and nonresonant parts of the nonlinear susceptibility.[32,40] Therefore either intensity maxima or points of inflection correspond to the resonant magnetic fields B_{res}. Whether extrema or points of inflection have to be evaluated, depends on the relative strengths of the resonant in comparison to the nonresonant contributions. Further details of the line-shape analysis of the CARS resonances are given in Refs. 32 and 42. If more transitions are close together, the exact resonance positions have to be found by a line-shape fitting taking into account real and imaginary parts of $\chi^{(3)}$.

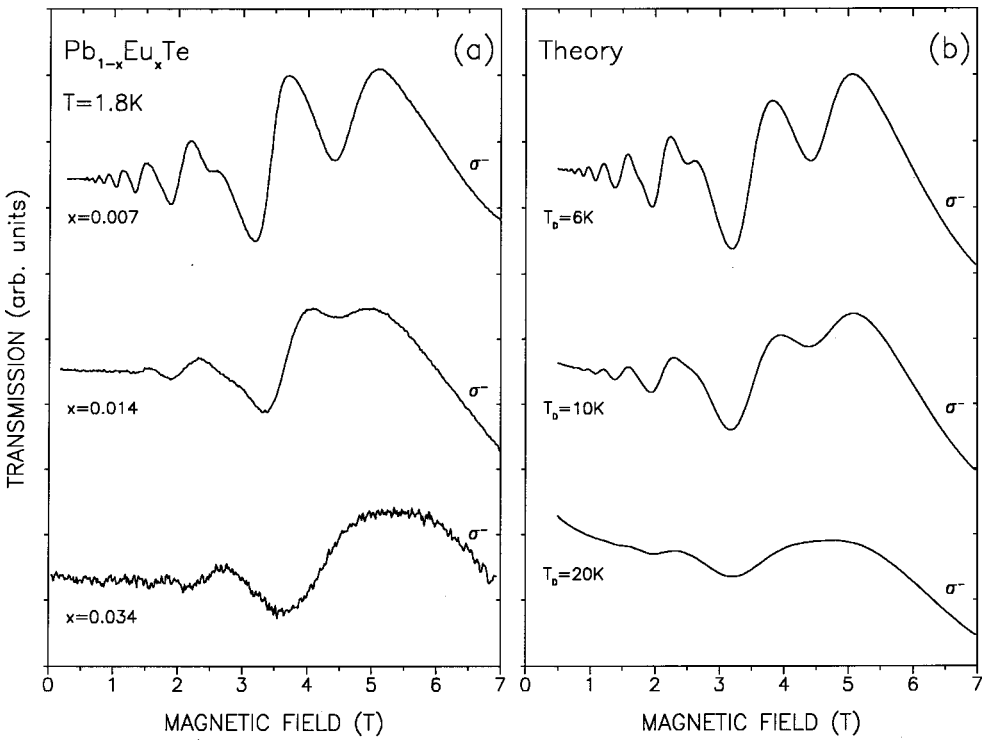

FIG. 3. (a) Interband magnetoabsorption of σ^- polarized radiation in three $Pb_{1-x}Eu_xTe$ samples with different Eu content vs magnetic field for $T=1.8$ K. $x=0.007$: $E_g=221.2$ meV, $\hbar\omega=260.4$ meV; $x=0.014$: $E_g=252.6$ meV, $\hbar\omega=285.2$ meV; $x=0.034$: $E_g=345.2$ meV, $\hbar\omega=375.1$ meV. (b) Calculated interband magnetoabsorption vs magnetic field for three different Dingle temperatures (band parameters from PbTe: $E_g=189.7$ meV, $\hbar\omega=236.2$ meV).

Figures 2(a) and 2(b) show experimental CARS recordings with fixed $\Delta\omega$ for small magnetic fields, where the valence-band spin splitting strongly depends on the magnetic field. In Fig. 2(a) a small splitting between the valleys with $\Phi=35.26°$ and 90.0° is observed; in the $Pb_{1-x}Eu_xSe$ sample with higher Eu content in Fig. 2(b) the splitting is not resolved due to the broader lines. Figure 2(c) shows a recording at fixed magnetic field in the range where the spin resonance is almost field independent. ω_L is held fixed and ω_S is tuned. The coherent Raman intensity is plotted vs the frequency difference $\Delta\tilde{\nu}$. A pronounced peak due to the valence-band spin resonance is observed at about 26 cm^{-1}. For small frequency differences an increase of the nonresonant susceptibility[43–45] occurs which is considered in the line-shape fitting procedure.

IV. EXPERIMENTAL RESULTS

A. Magneto-optical interband transitions

In Fig. 3(a) recordings of the transmitted intensities vs the magnetic field are compared for three $Pb_{1-x}Eu_xTe$ samples with different x values. The photon energies are chosen about 35 meV above the respective band gaps to allow a direct comparison of the curves. It is clearly seen that with increasing Eu content the linewidth is increased and the modulation is less pronounced. In Fig. 3(b) theoretical traces are shown for comparison, calculated by the method outlined in Sec. II C. The agreement of the shapes of calculated and experimental curves demonstrates that with increasing x the Dingle temperature is strongly enhanced due to alloy

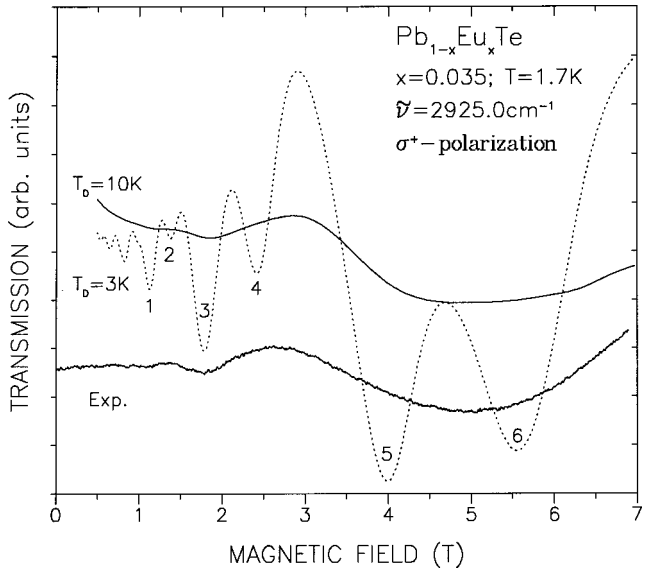

FIG. 4. Interband transmission of σ^+ polarized radiation in $Pb_{1-x}Eu_xTe$ with $x=0.035$ as a function of B (Faraday configuration, $T=1.8$ K). Full lower trace: Experiment; full upper trace: calculated with $T_D=10$ K; dotted trace: calculated with $T_D=3$ K (corresponding to the Dingle temperature in PbTe). The transitions are identified as 1: VB $2^-\rightarrow$CB 2^+, $\Phi=0.0°$ and VB $5^-\rightarrow$CB 5^+, $\Phi=70.53°$; 2: VB $4^-\rightarrow$CB 4^+, $\Phi=70.53°$; 3: VB $1^-\rightarrow$CB 1^+, $\Phi=0.0°$ and VB $3^-\rightarrow$CB 3^+, $\Phi=70.53°$; 4: VB $2^-\rightarrow$CB 2^+, $\Phi=70.53°$; 5: VB $1^-\rightarrow$CB 1^+, $\Phi=70.53°$; 6: VB $0^-\rightarrow$CB 0^+, $\Phi=0.0°$.

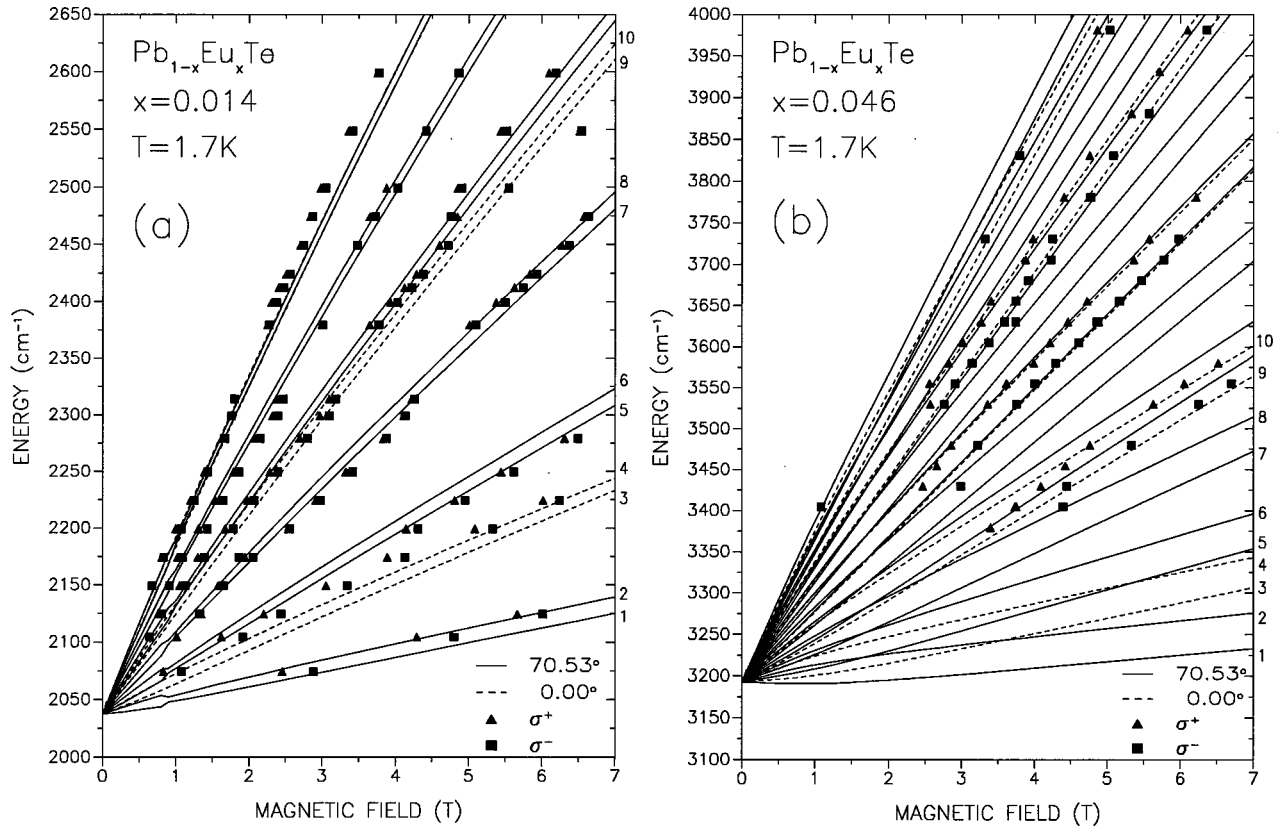

FIG. 5. Fan chart for magneto-optical transitions in Faraday geometry ($\mathbf{k}\|\mathbf{B}\|[111]$) for two $Pb_{1-x}Eu_xTe$ samples with $x=0.014$ (a) and $x=0.046$ (b). $T=1.7$ K. ▲: experimental results for σ^+ polarized radiation; ■: experimental results for σ^- polarized radiation; —, ---: calculated with parameters according to Table IV. Identification of the transitions: 1: $VB0^+\rightarrow CB0^-,\Phi=70.53°$; 2: $VB0^-\rightarrow CB0^+,\Phi=70.53°$; 3: $VB0^+\rightarrow CB0^-,\Phi=0.0°$; 4: $VB0^-\rightarrow CB0^+,\Phi=0.0°$; 5: $VB1^+\rightarrow CB1^-,\Phi=70.53°$; 6: $VB1^-\rightarrow CB1^+,\Phi=70.53°$; 7: $VB2^+\rightarrow CB2^-,\Phi=70.53°$; 8: $VB2^-\rightarrow CB2^+,\Phi=70.53°$; 9: $VB1^+\rightarrow CB1^-,\Phi=0.0°$; 10: $VB1^-\rightarrow CB1^+,\Phi=0.0°$.

scattering.[46,47] Weaker transitions (see, e.g., between 4 and 5 T) are no longer observable with higher Eu contents.

Figure 4 shows that this line broadening can cause only transmission minima remaining, where transitions with two valley orientations accidentally coincide (transition 3 at 4 T in Fig. 4) or relatively widely split transitions resulting in one broad minimum (between 4 and 6 T in Fig. 4). Consequently, from interband transmission the anisotropy of the matrixelements can no longer be deduced. Later we will show that CARS will provide this information. In samples where magnetotransmission does not at all show pronounced minima the energy gaps have been obtained by photoluminescence.

Fan charts of the dependence of interband transition energies as a function of the magnetic field are shown in Fig. 5 for $Pb_{1-x}Eu_xTe$ with different Eu contents. It is seen that with small x [Fig. 5(a)] all allowed transitions are resolved. For this sample E_g, $P_\perp$, and $P_\|$ can be fitted to interband data. As already mentioned above and seen from Fig. 5(b) this is no longer true for $x>4\%$. Transmission minima are only observed where transitions with $\Phi=0.0°$ and $\Phi=70.53°$ are close together. The spin splitting between σ^+ and σ^- transitions caused by the exchange interaction is more pronounced than with smaller x [compare Figs. 5(a) and 5(b)].

The full and broken lines are calculated with band and exchange parameters given in Table IV. The agreement between theory and experimental data is rather satisfactory. Similar results, which are not shown here, are obtained for the selenides.[5,6,16] The corresponding parameters are given in Table III.

B. Coherent Raman scattering

Experimental recordings of the CARS intensity vs. magnetic field are reproduced in Figs. 6(a) and 6(b) for p-type $Pb_{1-x}Eu_xTe$ with different Eu contents. In p-type material hole resonances are observed as well as resonances due to photoexcited electrons. Again a considerable line broadening with increasing x is seen, however, even in the sample with $x=0.046$ spin-flip transitions in valleys with $\Phi=35.26°$ and 90.0° are well resolved. To get exact resonance positions a careful line-shape analysis must be performed (the arrows give the resulting resonance positions).

Figure 6(a) demonstrates that the valence-band spin resonances show a pronounced temperature dependence, whereas the conduction band g factor remains constant. There is almost no exchange interaction between electrons and Eu^{2+} ions.[8] The exchange interaction between holes and Eu^{2+} is antiferromagnetic, which means with decreasing temperature the resonant magnetic field is enhanced—the spin splitting is diminished (higher resonant magnetic fields for constant $\Delta\omega$).

In Fig. 7 the spin splittings are plotted as a function of the magnetic field. The full lines are calculated with the band model outlined in Sec. II with band and exchange parameters

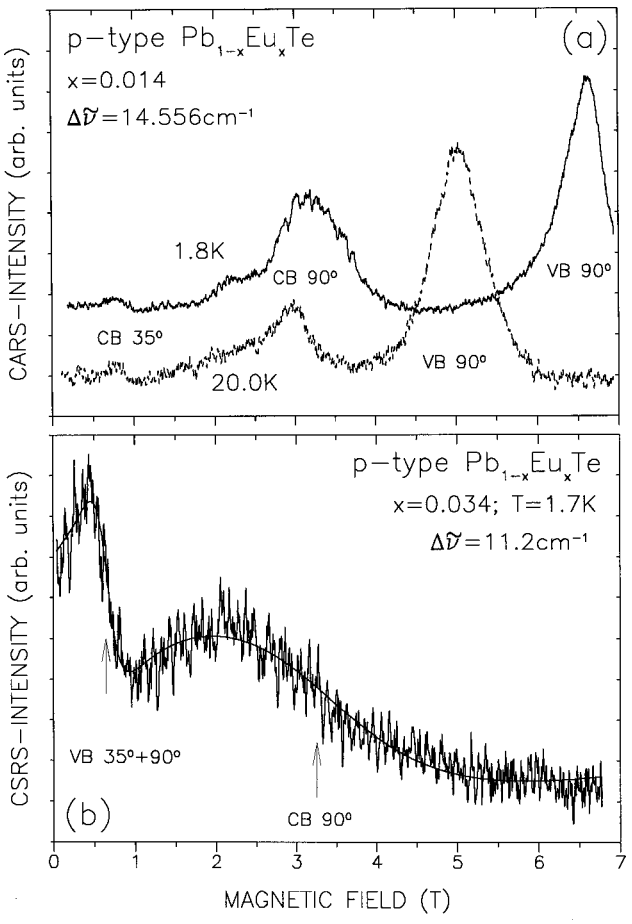

FIG. 6. CRS-intensity of p-type $Pb_{1-x}Eu_xTe$ with $x=0.014$ (a) and $x=0.034$ (b) as a function of the magnetic field for fixed frequency differences. The recordings for $T=1.8$ K and $T=20$ K exhibit a strong temperature dependence of the hole resonance in contrast to the electron resonances. The arrows in (b) denote the resonance positions obtained by a line-shape fitting (noise free trace).

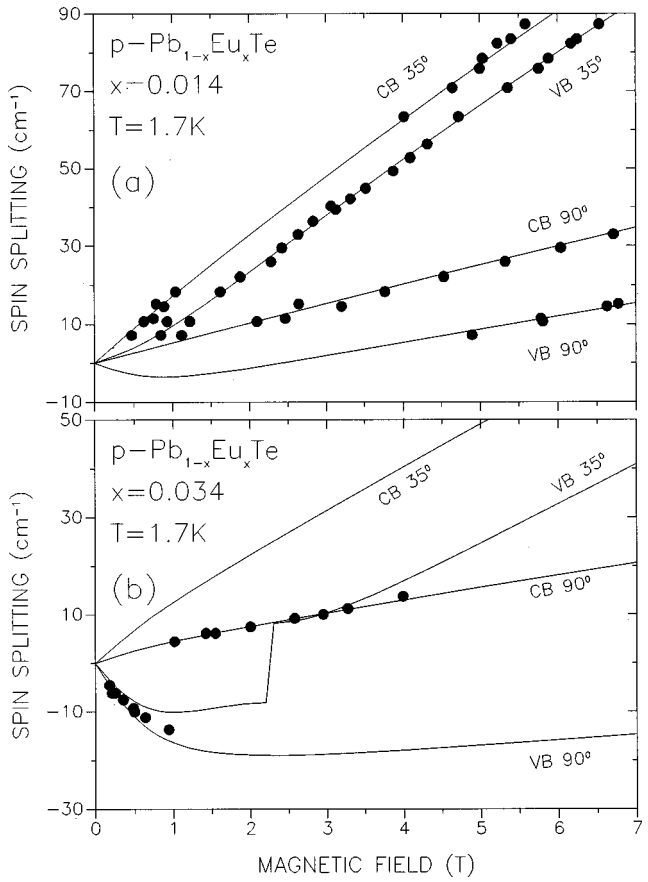

FIG. 7. Spin splittings vs magnetic field for p-type $Pb_{1-x}Eu_xTe$ with $x=0.014$ (a) and $x=0.034$ (b) for $T=1.7$ K. ●: experimental results; —: calculated with the parameters from Table IV.

fitted to interband and CARS data (see Table IV). The good agreement between calculated and experimentally observed spin splittings demonstrate the reliability of the exchange parameters.

Experimental CARS recordings for $Pb_{1-x}Eu_xSe$ are shown already in Fig. 2. Corresponding dependencies of the spin splittings as a function of the magnetic field are plotted in Fig. 8. Due to the weak magnetic-field dependence of the valence-band spin splitting in the sample with 6.9% europium, with fixed frequency lasers no results can be obtained between 1.5 T and 6 T. It is necessary to take the spectra at fixed magnetic field by tuning ω_S. The fitting procedure yielded for $x=0.042$ $T_0\approx 0$, whereas for $x=0.069$ $T_0=1.2$ K, demonstrating the onset of an antiferromagnetic coupling between the Eu^{2+} ions at this concentration (see also Refs. 24 and 30).

C. Discussion of band and exchange parameters

There is some controversy in literature concerning the interband matrix elements in $Pb_{1-x}Eu_xTe$. Krost *et al.*[10] found a decrease of the anisotropy with increasing Eu content. Karczewski *et al.*[11] published for one sample with $x=0.02$ $2P_\parallel^2/m_0=0.55$ eV, which is the PbTe value and $2P_\perp^2/m_0=8.23$ eV. This means an increase of the anisotropy. Yuan *et al.*[35] deduced from cyclotron resonances with electrons in the $\Phi=0°$ valley a decrease of $2P_\perp^2/m_0$ with increasing Eu content from $2P_\perp^2/m_0=5.3$ eV for $x=1.3\%$ to $2P_\perp^2/m_0=4.0$ eV for $x=3.4\%$. Yuan's results are obtained with samples which were also investigated by interband magnetotransmission. Thus the energy gaps of the samples are known very precisely. Since the conduction band is almost not affected by the exchange interaction, the anisotropy of the matrixelements is directly observed in the CARS spectra of n-type material.[8,9] There is no doubt, that the anisotropy $P_\perp/P_\parallel$ decreases with increasing Eu concentration (see Table IV).

Figure 9 gives a survey on the matrixelements in $Pb_{1-x}Eu_xTe$ and $Pb_{1-x}Eu_xSe$. In the telluride $2P_\perp^2/m_0$ as well as $2P_\parallel^2/m_0$ are reduced with respect to PbTe by a factor of approximately 2 for $x=0.05$, the effect being more pronounced for $P_\perp$ which leads to a decrease of the anisotropy with increasing x. In contrast, in the selenide there is just a very weak reduction of the matrixelements with increasing x (see Fig. 9 and Table III). Incidentally it should be noted that the same tendencies are found in $Pb_{1-x}Mn_xTe$ (Refs. 48 and 7) and $Pb_{1-x}Mn_xSe$,[32] respectively.

The different behavior of tellurides and selenides may be caused by the band alignment of the far bands. The energy differences between the far bands and the lowest conduction

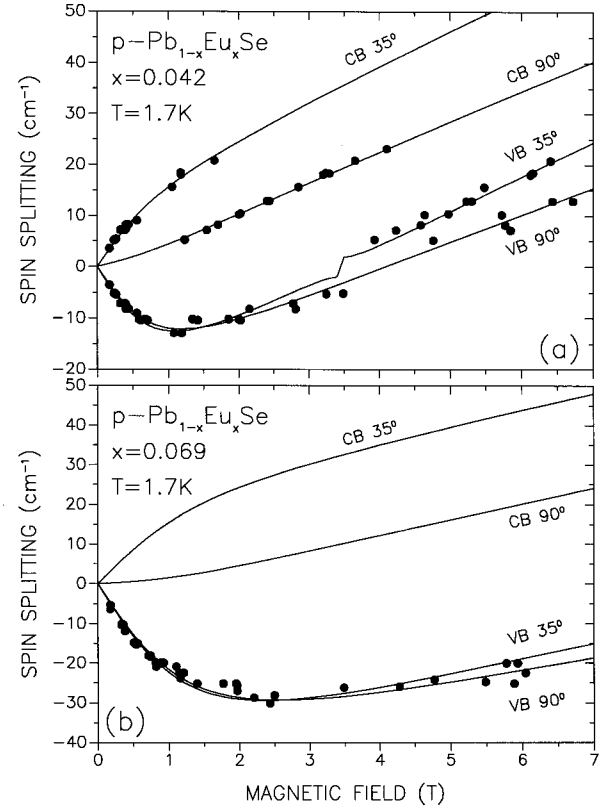

FIG. 8. Spin splittings vs magnetic field for p-type $Pb_{1-x}Eu_xSe$ with $x=0.042$ (a) and $x=0.069$ (b) for $T=1.7$ K. ●: experimental results; —: calculated with the parameters from Table III.

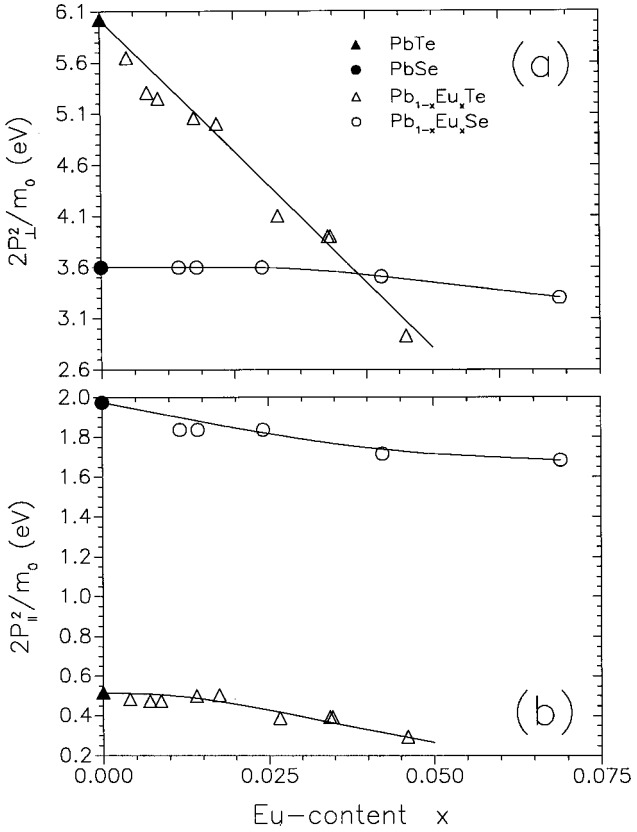

FIG. 9. Interband matrix elements $2P_\perp^2/m_0$ and $2P_\parallel^2/m_0$ of $Pb_{1-x}Eu_xTe$ and $Pb_{1-x}Eu_xSe$ as a function of the Eu content x. Full lines: guides for the eye. Data for $Pb_{1-x}Eu_xSe$, $x<0.025$ from Ref. 7.

and the highest valence band are smaller in PbTe (1–1.5 eV) than in PbSe (1.5–2 eV) and the conduction band shows a different band-edge symmetry.[13] Especially in $Pb_{1-x}Eu_xTe$ the energy gap opens quite drastically, so that this may cause the strong decrease of the matrix elements.

In the Mn-based diluted magnetic lead chalcogenides a dependence of some of the exchange parameters on x has been observed.[22] Such deviations of the molecular-field approximation are not found in the Eu compounds. All $Pb_{1-x}Eu_xTe$ samples yielded within the experimental errors the same exchange parameters (see Table IV). T_0 is treated as an adjustable parameter but remained equal to zero up to the highest Eu concentrations investigated. This points out that a considerable antiferromagnetic coupling between the magnetic moments of the Eu^{2+} ions does not occur. Therefore we assumed the effective spin to be $\frac{7}{2}$ for all samples in agreement with published magnetization data.[29,30]

In the selenide the data suggest a small decrease of exchange parameters with increasing Eu content (see Table

TABLE III. Band and exchange parameters of $Pb_{1-x}Eu_xSe$ for $T=1.8$ K. Far band parameters of PbSe from Ref. 51.

	PbSe (Ref. 51)	I	II	III	IV	V	VI
E_g (meV)	146.3 ±0.3	181.1	189.1	219.0	264.3	273.4	354.5
x	0.0	0.012	0.014	0.024	0.039	0.042	0.069
$2P_\perp^2/m_0$ (eV)	3.6 ±0.1	3.6	3.6	3.6	3.6	3.5	3.3
$P_\perp/P_\parallel$	1.35 ±0.02	1.4	1.4	1.4	1.4	1.4	
A (meV)			34±5	26±5	26±5	24±5	25±5
a_1 (meV)			32±5	22±5	20±5	20±5	23±5
B (meV)			7±5	20±5	8±5	12±5	
b_1 (meV)			8±5	19±5	1±5	3±5	
T_0 (K)		0.0	0.0	0.0	0.0	0.1	1.2
S_0		3.5	3.5	3.5	3.5	3.5	3.5

TABLE IV. Band and exchange parameters of $Pb_{1-x}Eu_xTe$ for $T=1.8$ K. Far band parameters of PbTe from Ref. 40.

	PbTe (Ref. 40)	*A*	*B*	*C*	*D*	*E*	*F*	*G*	*H*	*J*
E_g (meV)	189.7 ± 0.2	207.7	222.0	228.2	252.6	267.8	309.4	343.8	345.2	395.9
x	0.0	0.0040	0.0070	0.0086	0.014	0.017	0.027	0.034	0.035	0.046
$2P_\perp^2/m_0$ (eV)	6.02 ± 0.05	5.65	5.30	5.25	5.05	5.0	4.1	3.9	3.9	2.9
$P_\perp/P_\parallel$	3.42 ± 0.05	3.42	3.35	3.33	3.18	3.15	3.25	3.15	3.15	
A (meV)				26 ± 5					26 ± 5	
a_1 (meV)				24 ± 5					24 ± 5	
B (meV)				5 ± 5					5 ± 5	
b_1 (meV)				0 ± 3					-2.5 ± 3	
T_0 (K)						0.0				
S_0						3.5				

III), but the deviations are hardly bigger than the estimated experimental errors. T_0 remains zero up to $x=0.04$ and increases above 4% (see Table III). At $x=0.069$ an antiferromagnetic coupling of the Eu^{2+} ions manifests itself in $T_0=1.2$ K. Nevertheless we assumed $S_0=\frac{7}{2}$ even with 6.9% europium. There may be some reduction of S_0 in the samples with the highest Eu concentrations, which would cause an increase of the exchange parameters [see Eqs. (35) and (42) in Ref. 7]. To elucidate this point a comparison of our data to magnetization measurements performed at the same samples would be necessary, which are not available up to now.

A comparison of the exchange parameters of Se vs. Te compounds (Tables III and IV) shows that the effect of the Eu ions on the valence-band spin splittings is practically identical in both systems. In the conduction band, however, there is a difference. The conduction band of the selenide is affected by the exchange interaction [see also the Brillouin function like bending of the CB 35° curve in Fig. 8(a)]. In contrast, in the telluride the exchange parameters B and b_1 are vanishing within the experimental accuracy. Accordingly in Fig. 7(a) the curves CB 35° and CB 90° are linear despite a small bending due to nonparabolicity. These differences between selenide and telluride most probably stem from the different band-edge symmetries of the conduction bands in both materials (PbSe: L_{62}^-; PbTe: L_{63}^- in the notation after Ref. 13) resulting in different spin-orbit mixing parameters entering the conduction-band states [see Eqs. (9) and (10) of Ref. 7 and Eq. (1) and the following sentences of the present article].

Compared to Mn-based alloys the exchange integrals in the Eu compounds (see Table V) are a factor 10 smaller (compare to Ref. 49). The exchange interaction of the free carriers with the screened $4f$ electrons of the Eu^{2+} ions is much weaker than with Mn^{2+} $3d$ electrons. This trend is also obtained by Dietl *et al.*[50] in *ab initio* calculations using a microscopic tight-binding model of the spin-dependent coupling of free carriers and localized spins in the diluted magnetic alloys. The resulting exchange parameters are approximately a factor of 3 larger than the experimentally observed values, but the theoretical calculations confirm the signs and the relation between the exchange interaction in the valence and conduction band.

V. CONCLUSIONS

The magneto-optical interband absorption and coherent Raman-scattering experiments reported in this paper for $Pb_{1-x}Eu_xSe$ and $Pb_{1-x}Eu_xTe$ extend previous investigations to considerably higher Eu concentrations. These extensions as well as the large number of experiments carried out allow reliable statements on the dependence of both interband matrixelements $P_\parallel$ and $P_\perp$ on the Eu content up to more than 5%. In the investigated range of Eu contents, $Pb_{1-x}Eu_xTe$ retains the band symmetries at the L point of the Brillouin zone of PbTe and $Pb_{1-x}Eu_xSe$ that of the corresponding level ordering of PbSe. The interband matrixelements decrease considerably with increasing x in the telluride and remain almost constant in the selenide based system. The difference is most probably due to the different symmetry of the conduction-band states in the selenide in comparison to the telluride system.

Due to the large increase of the energy gap with increasing Eu content, in both systems alloy scattering is quite important and influences the line broadening of both interband

TABLE V. Exchange integrals of $Pb_{1-x}Eu_xTe$ and $Pb_{1-x}Eu_xSe$ for $T=1.8$ K.

Material	$\alpha=\langle R\|J\|R\rangle/\Omega_0$ (meV)	$\delta=\langle S_\pm\|J\|S_\pm\rangle/\Omega_0$ (meV)	$\beta_\perp=\langle Z_\pm\|J\|Z_\pm\rangle/\Omega_0$ (meV)	$\beta_\parallel=\langle X_\pm\|J\|X_\pm\rangle/\Omega_0$ (meV)
$Pb_{1-x}Eu_xSe$ $x=0.014$	33	-105	12	3
$Pb_{1-x}Eu_xTe$ $x=0.014/0.017$	25	-48	0	-7

and also to a somewhat lesser extent of the CARS spectra. The calculation of the interband transmission as a function of the magnetic field from the band and exchange parameters and its comparison with experimental recordings yields an increase of the Dingle temperature from $T_D \approx 3$ K in PbTe to approximately $T_D \approx 20$ K in $Pb_{1-x}Eu_xTe$ with 5% europium. For this reason the anisotropy of the matrix elements for higher Eu concentrations have to be determined by CARS measurements.

The exchange parameters in the Eu compounds are almost identical and about one order of magnitude smaller than in $Pb_{1-x}Mn_xSe$ and $Pb_{1-x}Mn_xTe$. In contrast to the Mn-based lead chalcogenides the exchange interaction decreases the valence-band spin splitting in $Pb_{1-x}Eu_xSe$ and $Pb_{1-x}Eu_xTe$. The conduction-band spin splitting in the telluride is not significantly affected by the exchange interaction with Eu, whereas there is a small effect in the selenide. The mechanism of the exchange interaction is discussed by Dietl *et al.*[50] and their theoretical calculations based on a microscopic tight-binding model of the spin-dependent coupling between the mobile carriers and the localized spins in the $Pb_{1-x}Eu_xSe$ and $Pb_{1-x}Eu_xTe$ compounds compare well in their trends with our experimental results.

Up to the highest Eu concentrations investigated here, the parameters describing the exchange interaction between localized magnetic moments and free carriers remain constant. Above $x = 0.05$ the onset of an antiferromagnetic coupling between the Eu^{2+} ions is suggested as evidenced from CARS data, namely T_0, the effective temperature entering the Brillouin function.

ACKNOWLEDGMENTS

We thank G. Meyer, P. Röthlein, and R. Schulz for making available unpublished data. The project was financially supported by Deutsche Forschungsgemeinschaft, Bonn, GME and FWF 11557, Vienna.

[1] M. Tacke, B. Spanger, A. Lambrecht, P. R. Norton, and H. Böttner, Appl. Phys. Lett. **53**, 2260 (1988).
[2] D. L. Partin, IEEE J. Quantum Electron. **QE-24**, 1716 (1988).
[3] A. Lambrecht, N. Herres, B. Spanger, S. Kuhn, H. Böttner, M. Tacke, and J. Evers, J. Cryst. Growth **108**, 301 (1991).
[4] D. L. Partin, in *Strained-Layer Superlattices: Materials Science and Technology*, edited by R. K. Willardson and A. C. Beer, Semiconductors and Semimetals Vol. 33 (Academic Press, New York, 1991), p. 311.
[5] P. Röthlein, G. Meyer, H. Pascher, and M. Tacke, *High Magnetic Fields in Semiconductor Physics II*, edited by G. Landwehr, Springer Series in Solid-State Sciences Vol. 87 (Springer-Verlag, Berlin, 1989), p. 573.
[6] P. Röthlein, H. Pascher, G. Bauer, and M. Tacke, Semicond. Sci. Technol. **5**, 147 (1990).
[7] G. Bauer, H. Pascher, and W. Zawadzki, Semicond. Sci. Technol. **7**, 703 (1992).
[8] F. Geist, H. Pascher, G. Springholz, and G. Bauer, in *Proceedings of the 7th International Conference on Narrow Gap Semiconductors, Santa Fe, New Mexico, 1995*, edited by J. C. Reno, IOP Conf. Proc. No. 144 (Institute of Physics and Physical Society, Bristol, 1995), p. 144.
[9] F. Geist, C. Mejia-Garcia, H. Pascher, G. Bauer, and G. Springholz, Mater. Sci. Forum **182-184**, 723 (1995).
[10] A. Krost, B. Harbecker, H. Schlegel, R. Faymonville, K. E. Ambrosch, and G. Bauer, J. Phys. C **18**, 2119 (1985).
[11] G. Karczewski, J. K. Furdyna, D. L. Partin, C. N. Trush, and J. P. Heremans, Phys. Rev. B **46**, 13 331 (1992).
[12] D. L. Mitchell and R. F. Wallis, Phys. Rev. **151**, 581 (1965).
[13] R. L. Bernick and L. Kleinman, Solid State Commun. **8**, 569 (1970).
[14] H. Yokoi, S. Takeyama, N. Miura, and G. Bauer, Phys. Rev. B **44**, 6519 (1991).
[15] H. Yokoi, S. Takeyama, O. Portugall, N. Miura, and G. Bauer, Physica B **184**, 173 (1993).
[16] C. Mejia-Garcia, Ph.D. thesis, University of Bayreuth, 1996.
[17] G. Bauer, *Narrow Gap Semiconductors, Physics and Applications*, edited by W. Zawadzki, Lecture Notes in Physics Vol. 133 (Springer-Verlag, Berlin, 1980), p. 427.
[18] W. C. Goltsos, A. V. Nurmikko, and D. L. Partin, Solid State Commun. **59**, 183 (1986).
[19] M. Iida, T. Shimizu, H. Enomoto, and H. Ozaki, Jpn. J. Appl. Phys., Part 1 **32**, 4449 (1993).
[20] J. A. Gaj, R. Planel, and G. Fishman, Solid State Commun. **29**, 435 (1979).
[21] J. Niedwodniczanska-Zawadzka, J. G. Elsinger, L. Palmetshofer, A. Lopez-Otero, E. J. Fantner, G. Bauer, and W. Zawadzki, Physica B & C **117&118B**, 458 (1983).
[22] H. Pascher, P. Röthlein, G. Bauer, and M. von Ortenberg, Phys. Rev. B **40**, 10 469 (1989).
[23] M. Gorska and J. R. Anderson, Phys. Rev. B **38**, 9120 (1988).
[24] V. Bindlatti, N. F. Oliveira, Jr., Y. Shapira, G. H. McCabe, M. T. Liu, S. Isber, S. Charar, M. Averous, E. J. McNiff, Jr., and Z. Golacki, Phys. Rev. B **53**, 5472 (1996).
[25] Shoichi Nagata, R. R. Galazka, D. P. Mullin, H. Akbarzadeh, G. D. Khattak, J. K. Furdyna, and P. H. Keesom, Phys. Rev. B **22**, 3331 (1980).
[26] R. R. Galazka and J. Kossut, *Narrow Gap Semiconductors, Physics and Applications* (Ref. 17), p. 245.
[27] M. Gorska and J. R. Anderson, Solid State Commun. **63**, 1055 (1987).
[28] J. R. Anderson and M. Gorska, Solid State Commun. **52**, 601 (1984).
[29] G. Braunstein, G. Dresselhaus, J. Heremans, and D. Partin, Phys. Rev. B **35**, 1969 (1987).
[30] M. Gorska, J. R. Anderson, G. Kido, and Z. Golacki, Solid State Commun. **75**, 363 (1990).
[31] J. Spalek, A. Lewicki, Z. Tarnawski, J. K. Furdyna, R. R. Galazka, and Z. Obuszko, Phys. Rev. B **33**, 3407 (1986).
[32] F. Geist, H. Pascher, N. Frank, and G. Bauer, Phys. Rev. B **53**, 3820 (1996).
[33] L. M. Roth, B. Lax, and S. Zwerdling, Phys. Rev. **114**, 90 (1959).
[34] L. M. Roth, and P. N. Agyres, in *Physics of III-V Compounds*, edited by R. Willardson and A. Beer, Semiconductors and Semimetals Vol. 1 (Academic, New York, 1966), p. 159.
[35] S. Yuan, H. Krenn, G. Springholz, Y. Ueta, G. Bauer, and P. J. McCann, Phys. Rev. B **55**, 4607 (1997).

[36] A. Ishida, S. Matsuura, M. Mizuno, and H. Fujiyasu, Appl. Phys. Lett. **51**, 478 (1987).
[37] R. E. Slusher, C. K. N. Patel, and P. A. Fleury, Phys. Rev. Lett. **18**, 77 (1967).
[38] H. Pascher, Semicond. Sci. Technol. **5**, 141 (1990).
[39] F. Geist and H. Pascher, J. Raman Spectrosc. **27**, 289 (1996).
[40] H. Pascher, Appl. Phys. B: Photophys. Laser Chem. **34**, 107 (1984).
[41] W. Hartig and W. Schmidt, Appl. Phys. **18**, 235 (1979).
[42] F. Geist, H. Pascher, M. Kriechbaum, N. Frank, and G. Bauer, Phys. Rev. B **54**, 4820 (1996).
[43] S. Y. Yuen and P. A. Wolff, Appl. Phys. Lett. **40**, 457 (1982).
[44] S. Y. Auyang and P. A. Wolff, J. Opt. Soc. Am. B **6**, 595 (1989).
[45] E. R. Youngdale, J. R. Meyer, F. J. Bartoli, and C. A. Hoffman, Int. J. Nonlinear Opt. Phys. **1**, 173 (1992).
[46] J. M. Ziman, *Electrons and Phonons* (Clarendon Press, Oxford, 1960).
[47] G. Bastard, *Wave Mechanics Applied to Semiconductor Heterostructures* (Les Editions de Physique, Les Ulis, France, 1988), p. 221.
[48] H. Pascher, P. Röthlein, G. Bauer, and L. Palmetshofer, Phys. Rev. B **36**, 9395 (1987).
[49] W. Hofmann, U. Fichtel, H. Pascher, N. Frank, and G. Bauer, Phys. Rev. B **45**, 8742 (1992).
[50] T. Dietl, C. Sliwa, G. Bauer, and H. Pascher, Phys. Rev. B **49**, 2230 (1994).
[51] H. Pascher, G. Bauer, and R. Grisar, Phys. Rev. B **38**, 3383 (1988).